IAEA-SM/366-122

MEASUREMENTS OF ENERGY SPECTRA IN THE NAC PROTON THERAPY BEAM

M.R. NCHODU[†], F.D. BROOKS, A. BUFFLER and M.S. ALLIE
Physics Department, University of Cape Town, Rondebosch, 7701 South Africa
D.T.L. JONES and J.E. SYMONS
Medical Radiation Group, National Accelerator Centre, Faure, 7131 South Africa

Abstract
A technique has been developed for measuring the energy spectra of high-energy proton therapy beams *in situ* under conditions similar to those used for radiotherapy. A thin polyethylene radiator is placed in the proton beam and two ΔE–E detector telescopes mounted outside the beam detect coincident proton pairs produced by p-p elastic scattering in the radiator. Measurements have been made to investigate the effect of standard beam modification elements on the energy spectrum of a proton therapy beam produced by a passive scattering system. Experimentally measured proton spectra are compared with simulated spectra calculated using the Monte Carlo code MCNPX.

1. INTRODUCTION

The nuclear particle therapy facilities of the South African National Accelerator Centre (NAC) are described by Jones *et al* [1] in another contribution to this meeting. The proton therapy facility that has operated at NAC since 1993 is based on a 203 MeV proton beam provided by a (k = 200) split-sector cyclotron. A radiotherapy beam is produced by directing the proton beam through a system of passive beam modification elements [2,3] such as scatterers, energy degraders, modulators and collimators, mounted immediately upstream of the patient treatment position. These devices modify the energy spectrum and other characteristics of the beam, and can thus be used to tailor the dose distribution delivered to the patient. Monte Carlo [4] and analytic [5,6] calculations may be used to predict the effect of different beam modification elements and thereby to achieve beam characteristics appropriate to specific treatment requirements. It is necessary that the results of these calculations should be validated by independent experimental measurements and measurements of the energy spectra of different proton therapy beams are valuable for this purpose. We have therefore developed a technique for measuring the spectra of proton therapy beams up to 200 MeV [7] and are using this technique to study proton therapy spectra at NAC.

2. THE PROTON SPECTROMETER

Treatment planning for proton therapy usually calls for a proton beam having an energy spectrum that is concentrated in a well-defined energy range. However, it is conceivable that beam modification systems may also introduce components at unwanted energies, for example low-energy "tails". It is therefore important that the experimental technique used to measure spectra should be capable of monitoring the spectrum accurately over a wide energy range and also a wide a range of intensity (eg 100:1). These requirements are unfortunately difficult to meet using "conventional" proton

[†] Present address: Dept. of Physics, University of the Western Cape, Bellville, 7535 South Africa

spectroscopy techniques, for example those based on traditional single-detector spectrometers such as NaI(Tl) scintillation crystals or large semiconductor detectors. At high proton energies (> 100 MeV) non-elastic nuclear interactions of protons on any high-Z material in the detector are significant and produce a so-called reaction tail which distorts the observed energy spectrum by enhancing the low energy component. Furthermore, severe electronic pile-up effects may occur if detectors are placed directly in a pulsed proton therapy beam such as that used at NAC. We have therefore used a completely different method, in which the proton beam falls on a thin hydrogenous radiator (polyethylene disc, 10 mm diam x 3 mm thick) and the energies of coincident proton pairs which result from p-p elastic scattering in the radiator are measured and summed to obtain the energy of the incident proton.

The experimental arrangement used (Fig. 1a) is a modified version of a design developed for previous studies of the NAC proton therapy beam [7]. Two detector telescopes, A and B, with axes at laboratory angles $\theta_A = \theta_B = 44.3°$ to the incident proton direction, detect the coincident proton pair. At non-relativistic incident proton energies (< 30 MeV) the kinematics of p-p elastic scattering (see Fig. 1b) dictate that the paths of the incident and outgoing protons be coplanar, that both θ_1 and θ_2 be < 90° and that $\theta_1+\theta_2 = 90°$. Relativistic effects become important as the incident proton energy increases and lead to a decrease in the laboratory angle between the two coincident protons. At E = 200 MeV, for example, $\theta_1+\theta_2$ reduces to 87.2°. The experimental geometry (Fig. 1a) ensures that this variation in the angle $\theta_1+\theta_2$ with proton energy does not affect the efficiency of the system for detecting coincident proton pairs. Each telescope incorporates three detectors: an active collimator AC consisting of a NE102A plastic scintillator slab, 8 cm x 6 cm x 5 mm thick, with a circular aperture at its centre; a ΔE-detector SD, consisting of a 1 mm thick x 20 mm diameter, totally-depleted semiconductor detector; and an E-detector LS, consisting of a NE213 liquid scintillator of diameter 45 mm, length 105 mm, with a thin (0.01 mm) aluminium entrance window for the incoming protons. The diameters of the collimator apertures of telescopes A and B are 4 and 10 mm respectively. At distances of 220 and 150 mm respectively from the centre of the radiator R (see Fig. 1a) the cones of acceptance for the two telescopes are therefore $\theta_A = 44.3 \pm 0.5°$ and $\theta_B = 44.3 \pm 1.9°$. For proton pairs from p-p elastic scattering at incident proton energies up to 200 MeV, the range of $\theta_1+\theta_2$ is $87.2° < \theta_1+\theta_2 < 90°$. Thus for every p-p scattered (or recoil) proton that is accepted by telescope A, the associated recoil (or scattered) proton will pass through the collimator aperture of telescope B and should be detected. In other words, geometrical factors will not introduce any variation of the efficiency for detecting p-p elastic scattering coincidences over this energy range.

The criterion for selecting events during experimental measurements was a four-fold, fast coincidence between the two LS detectors and the two SD detectors. Events in coincidence with a response from either of the two AC detectors were vetoed. Nine analogue signals were digitised by 12-bit ADCs for each accepted event and stored on disk (in list mode) for later off-line analysis. Four signals were taken from each telescope: the pulse heights from the SD and LS detectors and two pulse shape discrimination (PSD) signals from a Link Model 5010 pulse shape discriminator unit which was connected to LS. The ninth signal was a time-difference measurement between the outputs of the two telescopes, which was used for fine tuning of the fast coincidence selection. Cuts applied in the off-line analysis included, for each telescope, a ΔE-E cut (based on the SD and LS pulse heights) to select protons, a PSD cut to select protons in the LS-detector, and, for the coincidence between the two telescopes, a time-difference cut for the final coincidence selection. The pulse heights of the SD and LS detectors were calibrated to proton energy, making allowance for the (calculated) energy losses of protons in their travel, through air and other materials, from the radiator into LS. Using this calibration

the starting energies E_A and E_B of each proton pair were calculated directly from the pulse heights measured by the respective telescopes and, finally, the energy E of the incident proton was obtained from $E = E_A + E_B$.

3. MEASUREMENTS OF PROTON SPECTRA

Fig. 2 shows a two-parameter plot of counts per pixel as a function of the energies E_A and E_B, obtained when the radiator R (Fig.1) was positioned at the isocentre (treatment position) of the NAC proton therapy facility and irradiated by the "standard" NAC proton therapy beam of energy 190.8 MeV. The symmetry ($\theta_A \approx \theta_B$) of the experimental geometry (Fig. 1a) implies that the condition $E_A \approx E_B \approx 0.5E$ should be valid for detected proton pairs that originate from p-p elastic scattering in R. A large fraction of the events in Fig. 2 lie close to the diagonal $E_A \approx E_B$ and are thus consistent with this condition. The main exceptions are the small numbers of events that trail away from the dominant peak at $E_A \approx E_B \approx$ 95 MeV, either horizontally ($E_B \approx$ 95 MeV, $E_A <$ 95 MeV) or vertically ($E_A \approx$ 95 MeV, $E_B <$ 95 MeV). These components can be attributed to events which should have contributed to the dominant peak but are displaced by reaction tail effects (section 2) in the LS detector of one or other telescope, A or B. Reaction tail events can be suppressed by applying an additional two-parameter cut in the off-line analysis, as indicated by the dashed lines shown in Fig. 2, to select events which comply with the condition $E_A \approx E_B$.

Fig. 3 shows results obtained under the same conditions as Fig. 2 except that the energy of the proton beam was reduced to 91.9 MeV by introducing a graphite energy degrader at the entrance to the beam modification system. Reaction tail effects are less evident in this plot than in Fig. 2, as expected for the lower proton energy. However, the energy thresholds (about 29 MeV) of the two detector telescopes are clearly visible. It can be seen that these thresholds impose a threshold condition $E > E_{th}$ on the proton spectrum measurements, where $E_{th} \approx$ 60 MeV.

The energy distribution $N_D(E)$ of detected events that satisfy all of the off-line cuts mentioned above is related to the proton energy spectrum $N(E)$ by the equation

$$N_D(E) = \varepsilon(E)\, N(E) \qquad \ldots\ldots (1)$$

where $\varepsilon(E)$ represents the efficiency for producing and detecting a coincident proton pair from p-p elastic scattering in the radiator R. The spectrometer design ensures (section 2) that there are no geometrical factors that will contribute to the energy-dependence of $\varepsilon(E)$, therefore we assume that the variation of $\varepsilon(E)$ with E will be entirely due to the energy-dependence of the differential cross section for p-p elastic scattering, in other words the Rutherford cross section, which is proportional to $1/E^2$. Thus eqn, (1) may be rewritten

$$N(E) = k\, E^2\, N_D(E) \qquad \ldots\ldots (2)$$

where k is a constant. Since the purpose of the measurements is to determine only relative values of $N(E)$ the constant k has been arbitrarily adjusted, for each spectrum, so as to normalize the peak intensity of the spectrum to the value of 100 counts per energy bin.

Figure 4 shows: (a) the proton energy spectrum measured for an incident proton energy 190.8 MeV; and, (b) and (c), Monte-Carlo simulations of this spectrum calculated using the code MCNPX [8], (b) without, and (c) with, the resolution broadening introduced by the detection system folded into the calculation. Spectra (a) and (b) have been normalised to a peak value of 100 counts per bin. Spectrum (c) has been normalised to the same total proton count as spectrum (a). Spectra (a) and (c) of Fig. 4 are reproduced in Fig. 5 together with corresponding measured and simulated spectra for the proton therapy beam energies of 174.1, 134.6 and 91.9 MeV. As can be seen in Figs 4 and 5, the experimental measurements are in reasonable agreement with the Monte-Carlo calculations and confirm that the beam modification system is successful in controlling the proton energy spectrum over the range 90 – 200 MeV, as required for proton therapy, without introducing significant additional low energy components. However, it should be noted that the energy threshold of E_{th} = 60 MeV that applies to the experimental measurements precludes us from making any comment about the possibility of low energy components that may be present at energies below this level.

Figure 6 shows proton energy spectra measured using a 190.8 MeV proton beam, (a) without, and (b) with, a modulator propeller [2,3] incorporated in the beam modification system. Curve (c) of Fig. 6 shows the Monte-Carlo simulation of the experimentally measured spectrum (b). The modulator propeller [2] is a cylinder which rotates with its axis parallel to and alongside the beam, introducing a degrader of acrylic material of thickness varying between 0 and 50 mm as it rotates. This enables the energy spread of the proton spectrum to be increased in controlled way, when required for proton therapy. The results shown in Fig. 6 demonstrate that the propeller system is successful in producing a broader proton spectrum, as required, without introducing any significant, unwanted low energy component.

Low-energy components of the spectra may be conveniently displayed by calculating running integrals of the energy spectra, that is integrals *I(E)* of the number of events at energies between the detection threshold energy E_{th} and energy E, as a function of E, from $E = E_{th}$ to an arbitrary upper limit of 200 MeV,

$$I(E) = K \sum_{E_{th}}^{E} N(E) \qquad \ldots\ldots (3)$$

where K is a constant which is adjusted to normalize the limiting value of *I(E)* (at E = 200 MeV) to 100. Thus *I(E)* represents the percentage of the proton spectrum (above E_{th}) for which the proton energy lies within the range E_{th} to E. Fig. 7 shows the integrals *I(E)* calculated from the spectra (Fig. 5) measured for the beam energies 190.8, 174.1 and 134.6 MeV. For the spectrum measured using the 190.8 MeV proton beam, for example, the data in Fig. 7 show that about 6 % of the spectrum is due to protons of energy less than 176 MeV.

4. DISCUSSION AND CONCLUSIONS

Figs. 4–6 represent a small sample of the proton therapy beam spectra that have been investigated using the new technique. Studies have also been made of proton spectra obtained using different collimator geometries and at positions displaced from the isocentre both along and perpendicular to the beam axis. In order to carry out these measurements, the complete spectrometer (Fig. 1a), including radiator and detector telescopes, is mounted on a table which can be moved both along and at right

angles to the beam axis. Experimental measurements are being compared with Monte-Carlo simulated results, as in Figs. 4–6, for all configurations studied. No large discrepancies have been found yet between experimental data and the Monte-Carlo predictions.

Some unexpected results have also been obtained. For example, in Fig. 3, which shows data obtained using a proton therapy beam of energy 91.9 MeV, there is surprising evidence of a small number of events at proton energies *higher* than 91.9 MeV. This is demonstrated by the weak but distinct trail of events that extends, within the $E_A \approx E_B$ window, from the dominant (91.9 MeV) peak to about 200 MeV. Protons in this beam cannot have energy $E > 100$ MeV if they have passed through the graphite degrader at the entrance to the beam modification system. It may be conceivable that a very small fraction of the entering 203 MeV protons could somehow undergo multiple scattering along paths that bypass the graphite degrader and then return to a trajectory within the beam. However it is extremely unlikely that this could have happened in the beam modification system used at NAC. An alternative possibility might be $^{12}C(p,n)^{12}N$ reactions in the graphite degrader followed by n-p elastic scattering of forward-emitted neutrons in downstream components of the beam modification system. Further investigations will be undertaken to determine the source of this phenomenon. Although the proportion of high-energy protons in the data shown in Fig. 3 is very tiny (< 1%) it is obviously important to understand this phenomenon in view of the possible implications for proton therapy.

In summary, the proton spectrometer developed for this work, like the predecessor on which it is based [7], has been successfully tested and demonstrated, and is now being used to validate calculations of proton therapy spectra made using Monte-Carlo simulations. Such calculations are expected to become more widely used in the planning of proton therapy treatments in the future. The spectrometer has also proved useful in revealing unexpected features in the spectra of proton therapy beams.

REFERENCES

[1] D.T.L Jones, A.N. Schreuder, E.A. de Kock , J.E. Symons, A. O'Ryan and S. Schroeder, "Nuclear particle therapy at the South African National Accelerator Centre", contribution number IAEA-SM/366-123 to this meeting.

[2] D.T.L. Jones, A.N. Schreuder, J.E. Symons and M. Yudelev, "The NAC particle therapy facilities". *Hadrontherapy in Oncology*, edited by U. Amaldi and B. Larson. Amsterdam: Elsevier Science Publishers BV, 307-328, 1994.

[3] A.M. Koehler, R.J. Schneider, and J.M. Sisterson, "Range modulators for protons and heavy ions," *Nucl. Instr. Meth.* **131** (1975) 437-440.

[4] J.V. Siebers and M.M. Traynor, "Modeling of proton nozzles with LAHET Monte Carlo code," *J Brachyther. Int'l.* **13** (1997) 95-99.

[5] T. Bortfeld and W. Schlegel, "An analytical approximation of depth dose distributions for therapeutic proton beams," *Phys. Med. Biol.* **41** (1996) 1331-1339.

[6] A.K. Carlsson, P. Andreo and A. Brahme, "Monte Carlo and analytic calculation of proton pencil beams for computerized treatment plan optimization". *Phys. Med. Biol.* **42** (1997) 1033-1053.

[7] F.D. Brooks, D.T.L. Jones, C.C. Bowley, J.E. Symons, A. Buffler, and M.S. Allie, "Energy spectra in the NAC proton therapy beam", *Rad. Prot. Dosim.* **70** (1997) 477-480.

[8] H. G. Hughes, R.E. Prael and R.C. Little, "MCNPX - The LAHET/MCNP code merger", X-Division research note XTM-RN(U)97-012, LA-UR-97-4891, Los Alamos National Laboratory (April 1997).

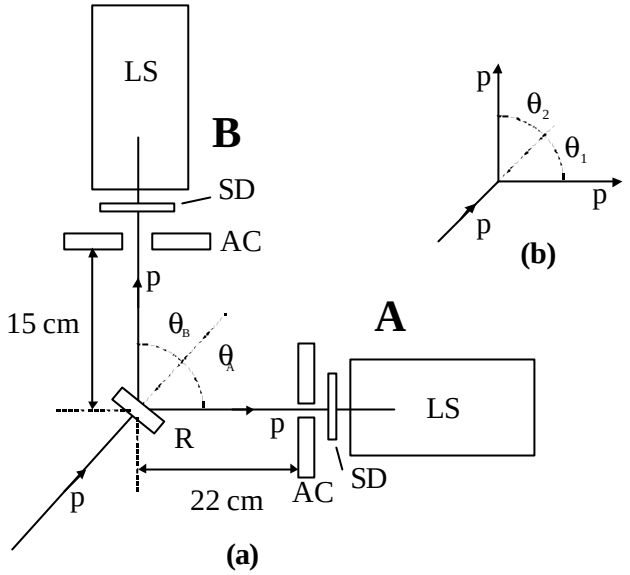

Fig. 1: (a) Schematic diagram of the proton spectrometer, showing polyethylene radiator (R), detector telescopes (A and B), active collimators (AC), semiconductor detectors (SD) and NE213 liquid scintillators (LS). (b) Schematic diagram of p-p elastic scattering

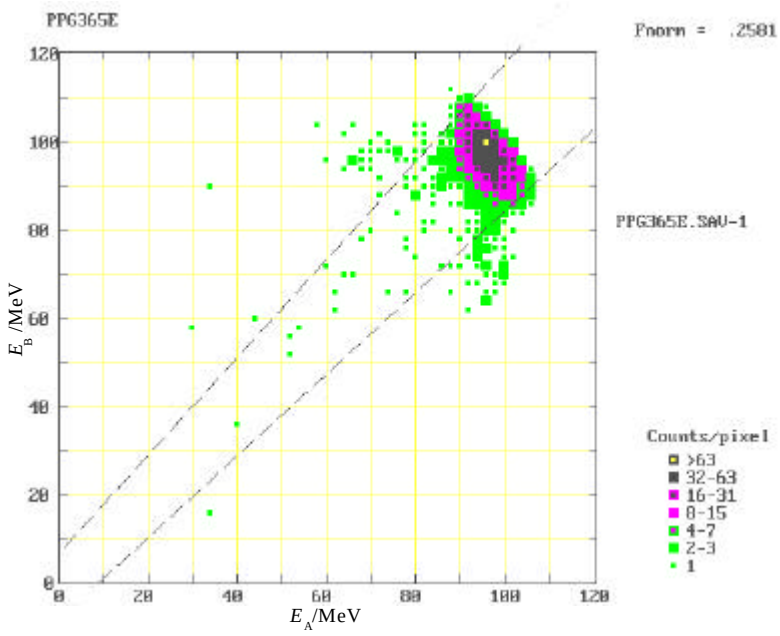

Fig. 2: Counts per pixel as a function of coincident proton energies E_A and E_B, measured using an incident proton beam of energy 190.8 MeV. The dashed lines show the boundaries of the cut used to select proton pairs from p-p elastic scattering in the radiator. Note that the counts scale is multiplied by a factor of 0.258.

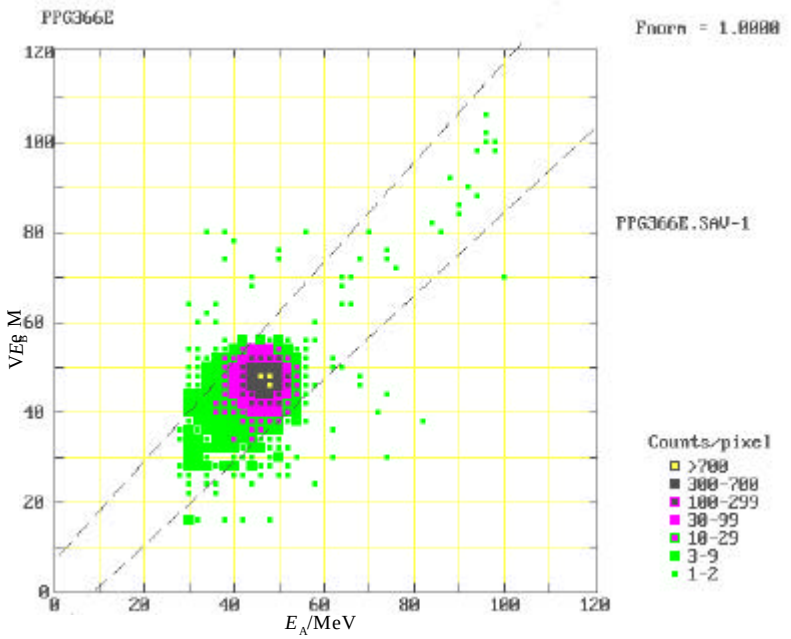

Fig. 3: Counts per pixel as a function of coincident proton energies E_A and E_B, measured using an incident proton beam of energy 91.9 MeV. The dashed lines show the boundaries of the cut used to select proton pairs from p-p elastic scattering in the radiator.

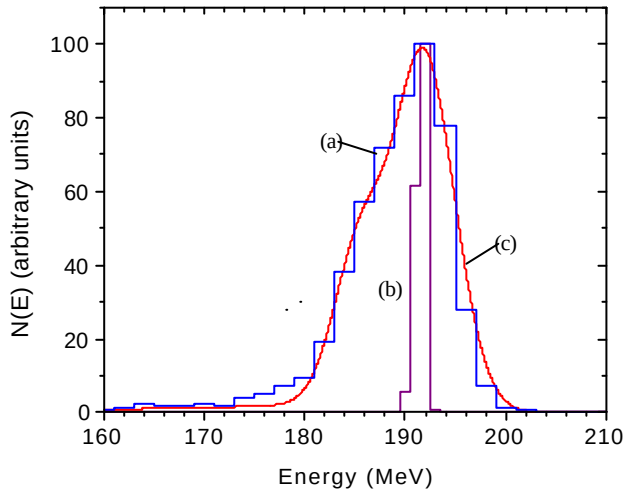

Fig. 4: Proton spectra *N(E)* measured and simulated for the 190.8 proton therapy beam: (a) measured spectrum (histogram); (b) spectrum simulated using MCNPX (histogram); and (c) spectrum (b) convoluted with the response function of the detection system (curve). Spectra (a) and (b) are normalized to a peak intensity of *N(E)* = 100. Spectrum (c) is normalized to the same total number of protons as (a).

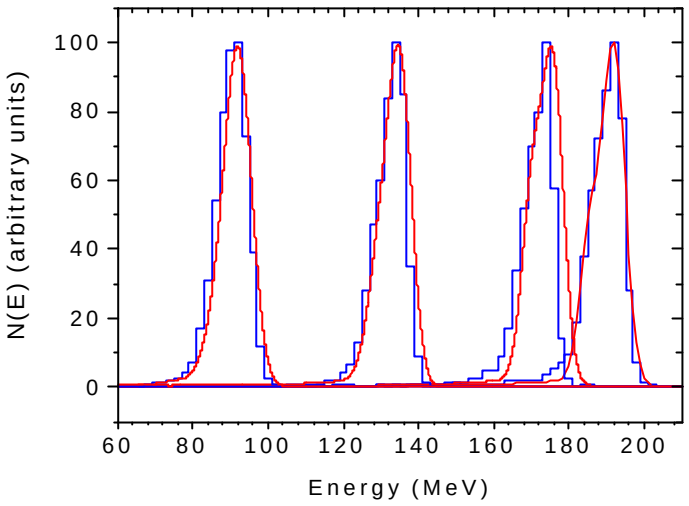

Fig. 5: Proton spectra as for (a) and (c) in Fig. 4 for proton beam energies of 91.9, 134.6, 174.1 and 190.8 MeV.

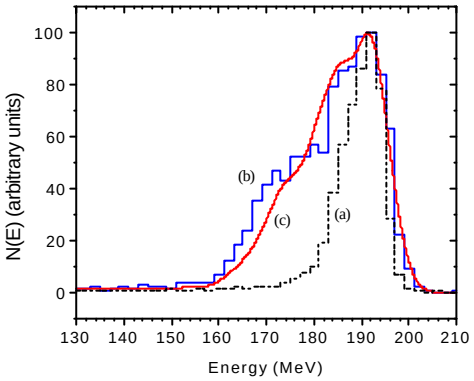

Fig. 6: Proton spectra for the 190.8 MeV proton therapy beam: (a) measured spectrum as in Fig. 4a; (b) measured spectrum as for (a) but with a 50 mm modulator propeller included in the beam modification system; and (c) simulated spectrum obtained using MCNPX for the conditions applying to (b).

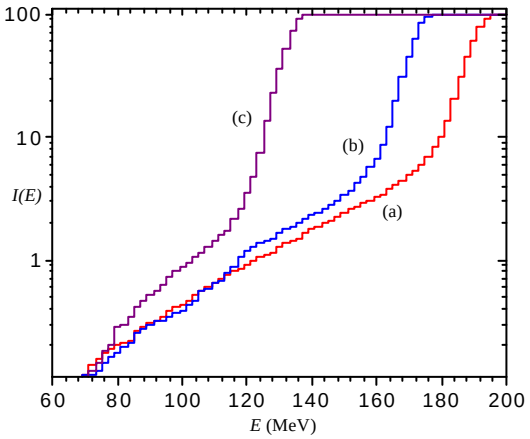

Fig. 7: Plot of the integral *I(E)* (eqn. (3)) for the spectra (Fig. 5) measured at proton beam energies of: (a) 190.8 MeV; (b) 174.1 MeV; and (c) 134.6 MeV.